

π -Bridge mediated coupling between inter- and intra-molecular charge transfer in aggregates for highly efficient near-infrared emission

Jingyi Xu¹ | Jie Xue¹ | Yu Dai¹ | Jinyuan Zhang² | Jiajun Ren³ | Chengyu Yao¹ |
Shaman Li¹ | Qingyu Meng¹ | Xueliang Wen¹ | Haoyun Shao¹ | Juan Qiao^{1,2,4} 

¹Key Lab of Organic Optoelectronics and Molecular Engineering of Ministry of Education, Department of Chemistry, Tsinghua University, Beijing, China

²Beijing National Laboratory for Molecular Sciences, CAS Key Laboratory of Organic Solids, Institute of Chemistry, Chinese Academy of Sciences, Beijing, China

³Key Laboratory of Theoretical and Computational Photochemistry, College of Chemistry, Ministry of Education, Beijing Normal University, Beijing, China

⁴Laboratory for Flexible Electronics Technology, Tsinghua University, Beijing, China

Correspondence

Juan Qiao, Key Lab of Organic Optoelectronics and Molecular Engineering of Ministry of Education, Department of Chemistry, Tsinghua University, Beijing 100084, China.

Email: qjuan@mail.tsinghua.edu.cn

Funding information

National Key R & D Program of China, Grant/Award Number: 2020YFA0715000;
National Natural Science Foundation of China, Grant/Award Number: 51773109

Abstract

Intermolecular charge transfer (inter-CT) is commonly considered to quench luminescence in molecular aggregates, especially for near-infrared (NIR) emission. Herein, by elaborate comparison of π -bridge effects in donor/acceptor (D/A) molecules, it is disclosed that a π -bridge is essential in D/A molecule to involve inter-CT in aggregates for inducing desired thermally activated delayed fluorescence (TADF) and largely suppressing non-radiative decays, and importantly, electron-donating π -bridge is critical to maximize radiative decay for inter-CT dominated emission by effective electronic coupling with bright intramolecular charge transfer (intra-CT) for high-efficiency NIR emission. As a proof-of-concept, TPATAP with thiényl as π -bridge realized prominent photoluminescence quantum yields of 18.9% at 788 nm in solid films, and achieved record-high maximum external quantum efficiencies of 4.53% at 785 nm in devices. These findings provide fresh insight into interplay between inter-CT and intra-CT in molecular aggregates and open a new avenue to attenuate the limitation of energy gap law for developing highly efficient NIR emitters and improving the luminescent efficiency of various inter-CT systems, such as organic photovoltaic, organic long persistent luminescence, etc.

KEY WORDS

intermolecular charge transfer, molecular aggregates, near-infrared emission, organic light-emitting diodes, thermally activated delayed fluorescence

1 | INTRODUCTION

The process of intermolecular charge transfer (inter-CT) holds fundamental significance across physical, chemical, and biological domains due to its multifaceted functionalities encompassing charge separation, transport and recombination.^[1–5] In recent years, inter-CT molecular system is playing a progressively pivotal role within the realm of materials science, manifesting extensive and promising applications in diverse fields such as organic light-emitting diodes (OLEDs),^[6] organic long persistent luminescence (OLPL),^[7] organic photovoltaic (OPV),^[8,9] organic field-effect transistors (OFET),^[10] photocatalysis,^[11] etc.

In light-emitting applications, exciplex systems exemplify evident inter-CT characteristic.^[12,13] By virtue of

nearly complete spatial separation between highest occupied molecular orbitals (HOMOs) and lowest unoccupied molecular orbitals (LUMOs), exciplex possesses innately minimal singlet-triplet energy splitting (ΔE_{ST}) values, facilitating the realization of desired thermally activated delayed fluorescence (TADF) emission through reverse intersystem crossing (RISC) process, and 100% exciton utilization in OLEDs.^[14] To date, blue and green exciplex OLEDs have attained external quantum efficiencies (EQEs) surpassing 20%,^[15] in stark contrast to near-infrared (NIR) exciplex OLEDs exhibiting inferior EQE of merely 1.24%.^[16,17] On one hand, according to Frank-Condon principle and Fermi's golden rule, large frontier orbital separation will lead to small transition dipole moments (μ) and oscillator strengths (f), and thus low radiative decay rates (k_r).^[18] On the other hand, the nonradiative decay rates (k_{nr}) would suffer exponential increase with the decrease of optical energy gap

Jingyi Xu, Jie Xue, Yu Dai and Jinyuan Zhang contributed equally to this work.

This is an open access article under the terms of the Creative Commons Attribution License, which permits use, distribution and reproduction in any medium, provided the original work is properly cited.

© 2024 The Author(s). Aggregate published by SCUT, AIEI, and John Wiley & Sons Australia, Ltd.

according to the well-known “energy gap law”.^[19] Consequently, the photoluminescence quantum yields (PLQY) of NIR-emitting exciplex systems with pure inter-CT characteristic are significantly diminished, thus leading to poor device performance.

In recent years, NIR organic emitters and OLEDs are in urgent need owing to their intrinsic flexibility and superb biocompatibility compared with inorganic counterparts, and have displayed promising applications in various fields such as night vision, optical communication, security authentication, biomedical imaging and phototherapy, etc.^[20–22] In order to achieve 100% internal quantum efficiencies (IQEs) in OLEDs, purely organic TADF materials without noble metals are more appealing. Except the above NIR exciplex systems, high-efficiency NIR TADF materials predominantly comprise twisted donor/acceptor (D/A) linked molecules exhibiting intrinsic intramolecular charge transfer (intra-CT) at single-molecule level.^[21,22] These D/A molecules generally possess large ground state dipole moment, facilitating the formation of closely packed dimers in aggregation state, thereby inducing inter-CT even at low doping concentrations.^[23–25] Moreover, it has been elucidated that the involvement of inter-CT exciton are highly desirable for NIR TADF materials due to numerous merits including significantly red-shifted emission, largely decreased ΔE_{ST} , enhanced TADF characteristic, and suppressed non-radiative processes by reducing non-adiabatic couplings.^[26–28] Hence, inter-CT aggregates have demonstrated promising potentials for mitigating the limitation of energy gap law. However, due to the conventionally perceived “dark” nature of inter-CT species for radiative emission owing to their vanishingly small f , the emission from those aggregates is more likely to be attributed to intra-CT rather than inter-CT states.^[24,29] More recently, we found high k_r can be achieved by effective electronic couplings between inter-CT and intra-CT states in molecular aggregates.^[25] In this work, we aim to unravel the prerequisites for this concerted inter-CT and intra-CT, and figure out the inner emission mechanism, together with universal molecular design strategies. It is well-recognized that aromatic π -bridges in D/A type molecules exert substantial influence on excited state characteristics and thereby optoelectronic properties,^[30,31] which is perfectly suitable for studying the interplay between inter-CT and intra-CT. To date, only few researches have investigated the influence of π -bridge on TADF materials and demonstrated some conflicting conclusions.^[32–34]

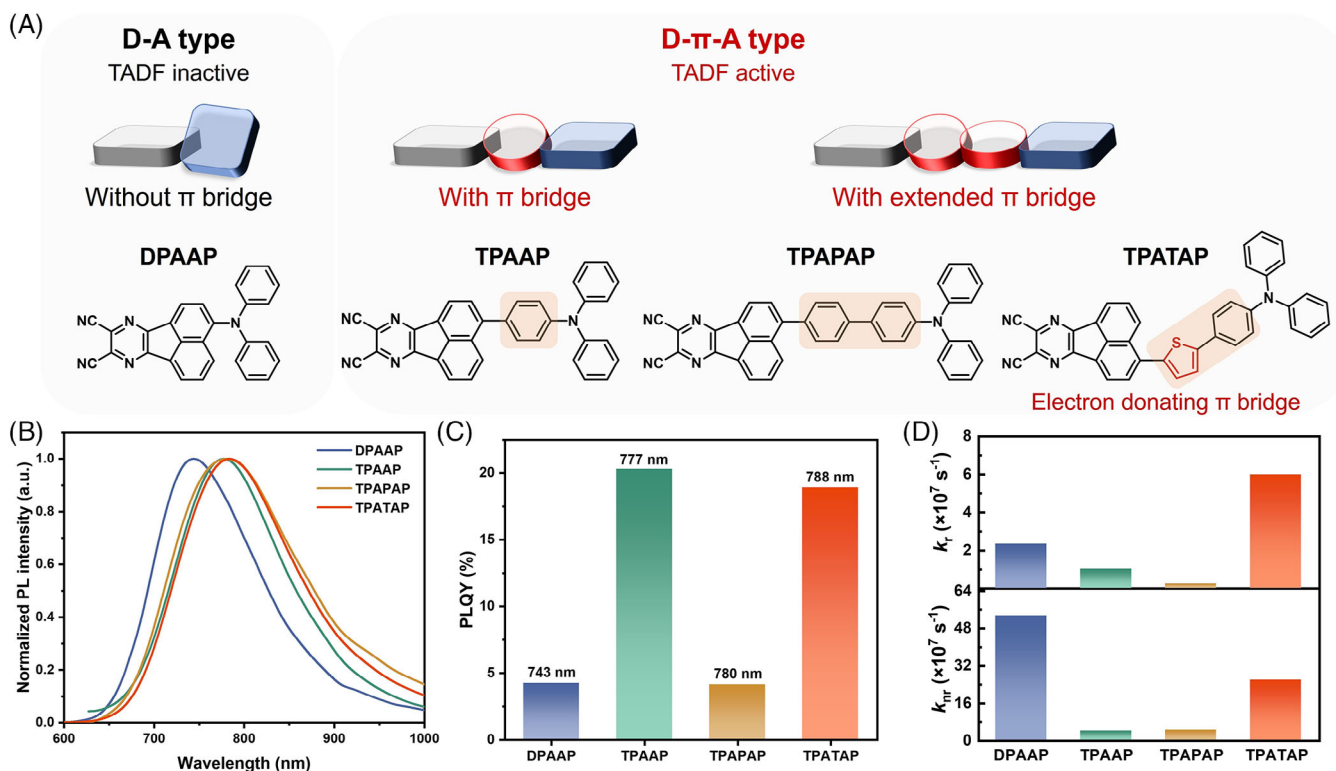
Herein, we rationally designed four D/A type compounds with different π -bridge based on widely used phenylamine type donors and acenaphtho[1,2-b]pyrazine-8,9-dicarbonitrile (AP) acceptor, and systematically investigated the relationship between π -bridge and their corresponding photophysical properties in single molecule and molecular aggregates. As shown in Scheme 1, the D-A type molecule DPAAP has no π -bridge, which is constructed by directly connecting diphenylamine (DPA) donor and AP acceptor. In comparison, the other three D- π -A type molecules, TPAAP, TPAPAP and TPATAP have different π -bridge. TPAAP is our previously reported TADF material which can form inter-CT aggregates and show the best OLED performance at that time with maximum external quantum efficiencies (EQEs) of 14.1% at 700 nm and 5.1% at 765 nm.^[26] Based on TPAAP, TPAPAP and TPATAP are

designed with an extra π -bridge, that is, phenyl and thiényl, respectively. The comprehensive comparison of this series of compounds would provide insights into the influence of π -bridge, not only with varying π -conjugation length, but also with different electronic characteristic. Two major prerequisites are disclosed to achieve high PLQY in solid states for NIR TADF. First, a π -bridge is essential in D/A type molecule to possess inter-CT characteristic in aggregation state for inducing TADF and suppressing k_{nr} . Second, electronically active π -bridge in HOMO distributions is more favorable for maximizing k_r in inter-CT dominated emission by effective electronic coupling with intra-CT states. Meanwhile, the introduction of a longer π -bridge could further enhance horizontal emitting dipole orientation ratio ($\Theta_{//}$) and optical outcoupling efficiency for OLEDs. Consequently, TPATAP with electron-rich thiényl as an extra π -bridge satisfies all the required conditions, which simultaneously achieves significant emission redshift, superior PLQY values and enhanced $\Theta_{//}$ in solid states, finally delivering outstanding performances in NIR-OLEDs. The maximum EQEs are 4.53% at 785 nm and 1.26% at 835 nm, representing the state-of-the-art performances among NIR OLEDs above 780 nm based on TADF emitters. The vital π -bridge effect revealed here provides fresh insight into how interplay between inter-CT and intra-CT in molecular aggregates, which will not only give valuable guidance for the development of highly efficient NIR TADF materials, but also have important implications for various fields in materials science involving inter-CT states.

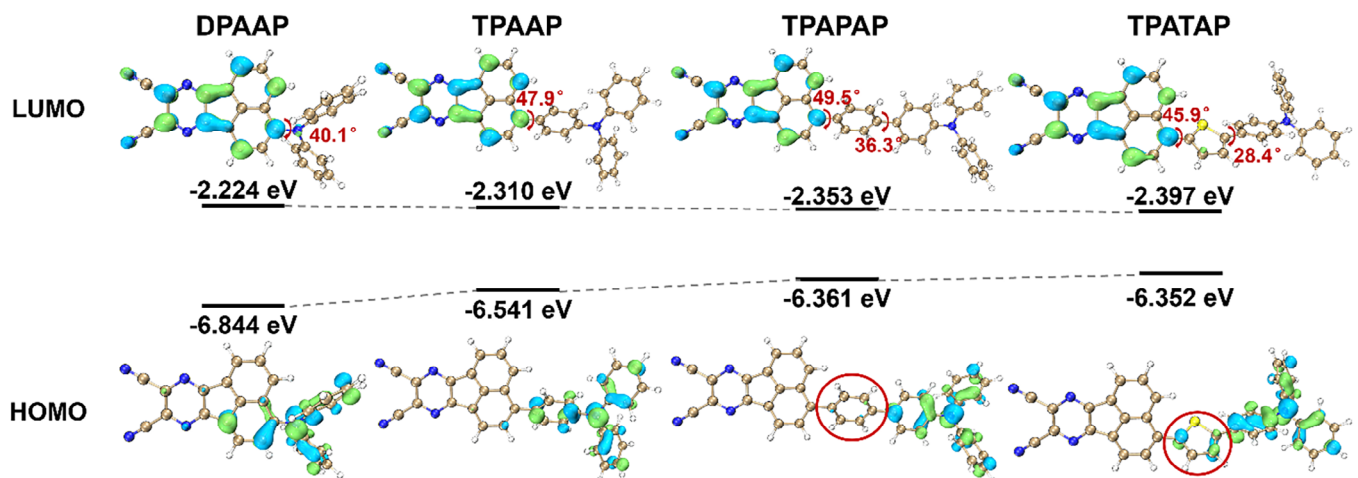
2 | RESULTS AND DISCUSSION

2.1 | Theoretical calculations of single molecule

To explore the relationship between molecular structure and electronic properties upon regulating π -bridge, we performed theoretical calculations using density functional theory (DFT) and time-dependent DFT (TD-DFT) at the level of M06-2X/6-31 g(d). As shown in Figure 1, the LUMO distributions of these molecules all locate in the acceptor part, while their HOMO distributions vary greatly. For DPAAP, the HOMO distributes in both DPA donor and adjacent benzene ring in AP, owing to direct connection of nitrogen atom to AP acceptor with a relatively small D/A dihedral angle of 40.1°. From DPAAP to TPAAP, the introduction of one phenyl bridge increases dihedral angle between AP and phenyl bridge to 47.9° due to larger steric hindrance, leading to its HOMO mostly localizes on the triphenylamine (TPA) donor. Meanwhile, the stronger electron-donating capability of TPA also leads to a distinct elevation of HOMO energy levels. From TPAAP to TPAPAP, although one more phenyl is introduced into the π -bridge, the HOMO of TPAPAP still locates on TPA part, indicating the additional phenyl π -bridge adjacent to AP mainly extends π -conjugation length and further destabilizes HOMO energy level of TPAPAP. From TPAAP to TPATAP, when replacing the π -bridge to electron-rich thiényl, the HOMO expands to both TPA and thiényl, demonstrating the insertion of thiényl π -bridge not only increases π -conjugation length, but also enhances electron-donating capability of the donor part, leading to the highest HOMO



S C H E M E 1 (A) Illustration of D-A and D- π -A designs explored in this study, as well as molecular structures of DPAAP, TPAPAP and TPATAP compared with TPAAP. Their (B) PL spectra, (C) PLQY, (D) k_r and k_{nr} values in solid films with comparable emission peak wavelength (neat films for DPAAP, TPAAP, TPAPAP, and 60 wt% doped film for TPATAP).



F I G U R E 1 Optimized molecular geometries of ground state with dihedral angels, calculated HOMO, LUMO distributions (isovalue = 0.02) and energy levels.

energy level for TPATAP. Meanwhile, the LUMO energy level is slightly stabilized from DPAAP to TPATAP.

As to the properties of excited states, from DPAAP to TPAPAP, the S_0-S_1 vertical transition energy (E_{S_1}) displays a gradual increase from 2.881 to 3.188 eV. Compared with TPAPAP, the electron-donating thiényl π -bridge in TPATAP significantly decreases E_{S_1} to 2.916 eV. With regard to f , D-A type molecule DPAAP possesses the smallest f of 0.400, and D- π -A type molecules TPAAP and TPAPAP possess larger f of 0.577 and 0.517, respectively. The largest f of 0.726 is realized in TPATAP due to strong electron-donating capability of thiényl and small dihedral angle between thiényl π -bridge and AP acceptor (details in Supporting Information). In comparison to TPATAP, molecules based on pyridinyl π -bridge

with electron-withdrawing properties display increased excitation energy and reduced f (Figure S2), which is undesirable for achieving high efficiency and long wavelength NIR emission. For ΔE_{ST} values, compared with DPAAP, D- π -A type molecules display smaller ΔE_{ST} with a decrease around 0.1–0.15 eV due to more effective HOMO/LUMO separation.

2.2 | Synthesis, characterization and single-crystal structures

DPAAP, TPAPAP and TPATAP were synthesized in good yields utilizing well-established reaction routes including Buchwald–Hartwig cross-coupling, Suzuki–Miyaura

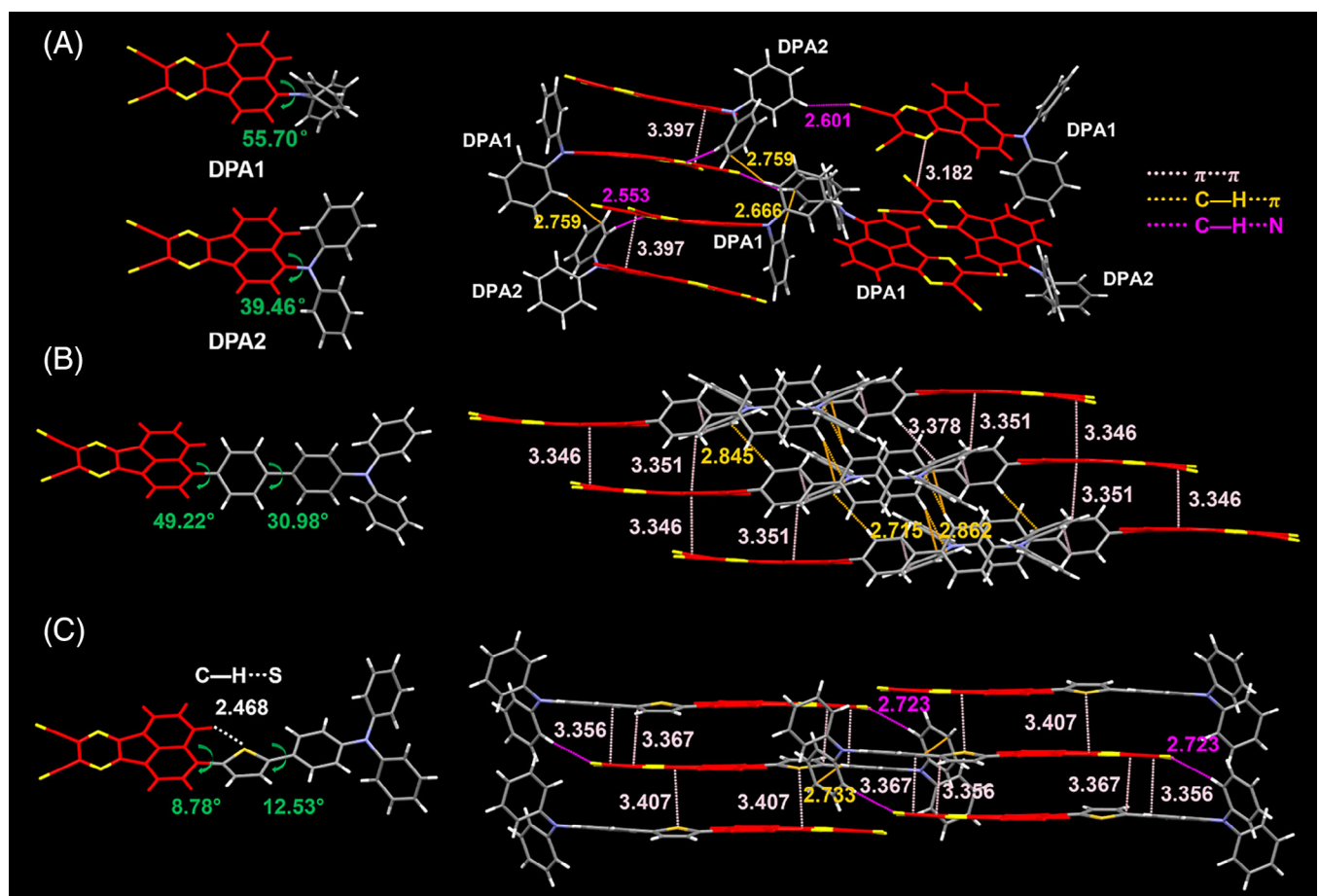


FIGURE 2 Molecular structures and packing patterns of (A) DPAAP, (B) TPAPAP and (C) TPATAP in single crystals.

cross-coupling, Miyaura borylation and dehydration condensation reactions. The final products were further purified by temperature-gradient vacuum sublimation, and fully characterized by $^1\text{H-NMR}$, $^{13}\text{C-NMR}$ spectroscopy, and high-resolution MALDI-TOF mass spectrometry (details in Supporting Information).

The single crystals of DPAAP, TPAPAP and TPATAP were readily obtained during sublimation, and relevant crystal data were summarized in Table S1. For DPAAP, there are two molecular configurations owing to the distortion of DPA, with different dihedral angles of 55.70° and 39.46° between D/A subunits for DPA1 and DPA2, respectively (Figure 2A). The planar acceptor parts tend to overlap with each other through $\pi\cdots\pi$ interactions (3.397 \AA), in an inclined pattern along the longitudinal axis of the molecule. Meanwhile, compared with TPAAP, the smaller DPA donor structure also leads to fewer intermolecular interactions in long-range packing of DPPAP single crystals.

In TPAPAP single crystals, the dihedral angles are 49.22° between AP and phenyl π -bridge, and 30.98° between phenyl π -bridge and TPA (Figure 2B), in good agreement with theoretical calculations (49.5° and 36.3° in gas phase). The π -bridge extension brings about abundant intermolecular interactions between neighboring donors through multiple C-H··· π interactions, meanwhile the AP acceptor part displays stronger $\pi\cdots\pi$ interactions (3.346 \AA) with adjacent AP and a little weaker $\pi\cdots\pi$ interactions (3.351 \AA) with phenyl π -bridge. In long-range packing, TPAPAP molecules adopt staggered staircase pattern along the transverse axis of the molecule, and the intermole-

cular interactions are mainly between D-D part and A-A part.

In TPATAP single crystals, the molecule exhibits largely reduced dihedral angles of 8.78° between AP and thienyl π -bridge, and 12.53° between thienyl π -bridge and TPA (Figure 2C), which is very different from the calculated results (45.9° and 28.4° in gas phase). This phenomenon could be ascribed to much denser packing in single crystal as evidenced by the highest density of 1.385 g cm^{-3} , leading to a shortened intramolecular hydrogen bond (C-H···S) length from 2.694 \AA in gas phase to 2.468 \AA in single crystal. Meanwhile, the largely reduced dihedral angles also give rise to more intermolecular interactions between thienyl π -bridge and AP acceptor through multiple $\pi\cdots\pi$ interactions, avoiding direct stacking between AP acceptors. For long-range packing, two TPATAP molecules firstly form dimer in an antiparallel head-to-tail fashion by $\pi\cdots\pi$ interactions (3.364 \AA) between thiophene and AP, and multiple C-H···N hydrogen bonds (2.723 \AA and 3.356 \AA) between the ending phenyl group and cyan group, and then dimers pack up along the vertical direction through a little weaker $\pi\cdots\pi$ interactions (3.407 \AA).

2.3 | Photophysical properties

Photophysical properties at single-molecule level were firstly investigated in dilute solutions. Similar to TPAAP, the other three compounds also exhibit two major absorption bands in oxygen-free toluene (Figure 3A). The absorption band

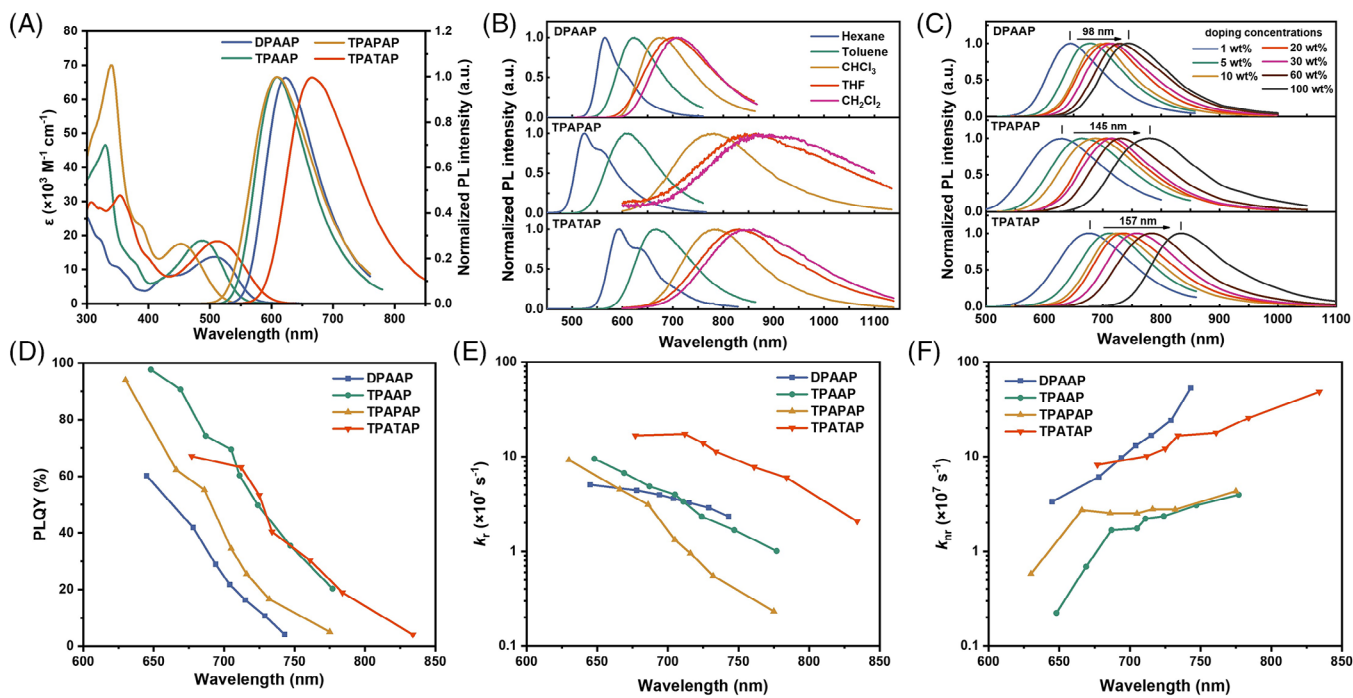


FIGURE 3 (A) Absorption and PL spectra in dilute oxygen-free toluene ($1 \times 10^{-5} \text{ mol L}^{-1}$) of DPAAP, TPAPAP and TPATAP compared with TPAAP. (B) PL spectra of DPAAP, TPAPAP and TPATAP in solutions with different polarity. (C) PL spectra of DPAAP, TPAPAP and TPATAP doped films with TPB as host at various doping concentrations. (D–F) The variation trends of PLQY, k_r and k_{nr} as a function of emission wavelength compared with TPAAP.

TABLE 1 Photophysical characteristics of DPAAP, TPAPAP and TPATAP in solutions with the comparison with TPAAP.

Compound	$\lambda_{abs,CT}^{a)}$ [nm]	$f_{exp}^{a,b)}$	$\lambda_{em}^{a)}$ [nm]	PLQY ^{a)} [%]	$\tau^{a)}$ [ns]	$k_r^{a)}$ [$\times 10^8 \text{ s}^{-1}$]	$k_{nr}^{a)}$ [$\times 10^7 \text{ s}^{-1}$]	$\Delta E_{ST}^{c)}$ [eV]
DPAAP	509	0.227	624	90.0	10.0	0.90	1.01	0.31
TPAAP	487	0.304	609	97.3	6.90	1.41	0.39	0.19
TPAPAP	453	0.278	609	96.7	6.95	1.39	0.48	0.20
TPATAP	513	0.371	666	93.0	3.74	2.49	1.87	0.19

^{a)}Measured in oxygen-free toluene solution ($1 \times 10^{-5} \text{ mol L}^{-1}$) at room temperature.

^{b)}Obtained experimentally.

^{c)}Measured in toluene solution ($1 \times 10^{-5} \text{ mol L}^{-1}$) at 77K.

below 400 nm is ascribed to the localized $\pi-\pi^*$ transitions of conjugated skeletons, and moderate broad absorption band above 420 nm is assigned to intra-CT transitions. The CT absorption peak wavelengths ($\lambda_{abs,CT}$) are 509, 487, 453 and 513 nm for DPAAP, TPAAP, TPAPAP and TPATAP, respectively (Table 1). Through the integral of intra-CT absorption band, the experimental f_{exp} could be determined by:^[35,36]

$$f_{exp} = 4.3 \times 10^{-9} \int \varepsilon \, d\nu \quad (1)$$

where ε is the molar extinction coefficient, ν is the wavenumber of absorption. The f_{exp} values are in ascending order for DPAAP, TPAPAP, TPAAP and TPATAP, with value of 0.227, 0.278, 0.304 and 0.371, respectively.

Similar to TPAAP, DPAAP, TPAPAP and TPATAP show no TADF in oxygen-free toluene and their PL lifetimes are 10.0, 6.95 and 3.74 ns, respectively. Among four compounds, DPAAP displays red emission ($\lambda_{em} = 624 \text{ nm}$, Figure 3A) with the lowest PLQY of 90.0%, due to the lowest k_r originated from the smallest f , and a higher k_{nr} originated from the largest reorganization energy λ_s (Figure S3) together with increased non-radiative processes induced by N=C

bond twisting and stretching, that is, free rotor and loose bolt effects.^[37,38] Compared with TPAAP, TPAPAP displays identical orange emissions with λ_{em} at 609 nm, but a little lower PLQY due to a lower f and k_r , together with a higher λ_s and k_{nr} . TPATAP exhibits a large red-shift to deep red emission with λ_{em} at 666 nm, but still maintains a remarkably high PLQY of 93.0% due to greatly increased k_r , which is the highest PLQY value among reported TADF molecules in the same spectral range.^[39–41]

According to S_1 and T_1 state energies determined by low temperature fluorescence and phosphorescence spectra at 77 K (Figure S5), ΔE_{ST} values of DPAAP, TPAPAP and TPATAP are calculated to be 0.31, 0.20 and 0.19 eV in toluene, respectively, the latter two are almost the same as that of TPAAP. Besides, upon increasing solvent polarity, these three compounds exhibit positive solvatochromic effect like TPAAP, indicating typical intra-CT characteristic (Figure 3B). However, from non-polar hexane to high polar dichloromethane, their bathochromic shift degree is quite different, that is, 146, 356 and 252 nm for DPAAP, TPAPAP and TPATAP, respectively, which could be rationalized by calculated distance between hole and electron centroid ($d_{h/e}$) and

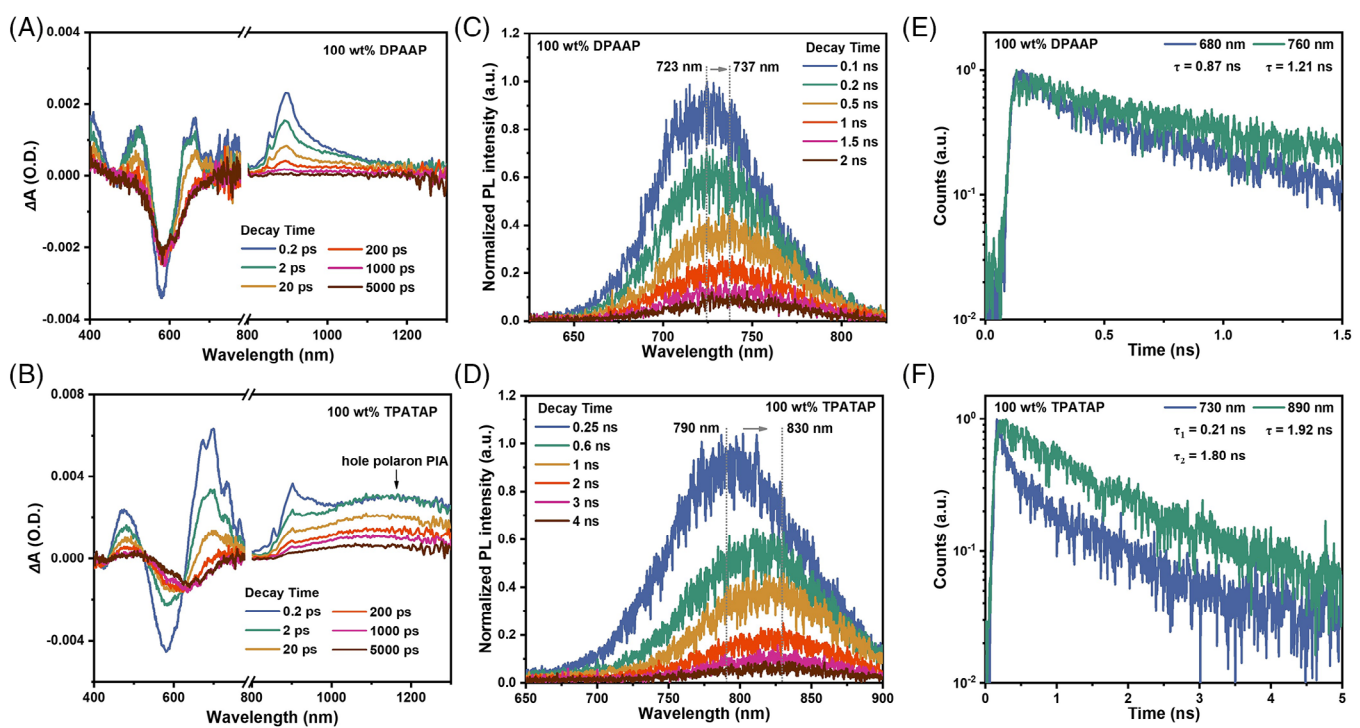


FIGURE 4 (A,B) Transient absorption spectra of DPAAP and TPATAP neat film, respectively. The disconnect in the spectral data is due to the gap in probe range around 800 nm. (C,D) Time-resolved PL measurements and (E,F) decay profiles of DPAAP and TPATAP neat film, respectively.

excited state dipole moment μ at single-molecule level (Table S2). Large $d_{h/e}$ and μ values in S_1 state allow a higher sensitivity to external polar environment, which is the case in TPATAP with the biggest solvatochromic effect.

To further explore aggregation effect, solid-state photophysical properties of DPAAP, TPAPAP and TPATAP in 2,2',2''-(1,3,5-benzenetriyl)-tris(1-phenyl-1-H-benzimidazole) (TPBi) host at different weight concentrations were examined through steady state and transient state spectroscopies. From 1 to 100 wt%, their CT absorption peaks exhibit progressive bathochromic shift (Figure S6), and their PL spectra exhibit more significant emission peak bathochromic-shift (Figure 3C). DPAAP solid films show the smallest PL redshift degree due to the lowest dipole moment μ and CT ratio in S_1 state. The T_1 energies of doped films also exhibits gradual decrease upon increasing doping concentrations (Tables S3 to S5 and Figures S7 to S9), but to a lesser extent compared with S_1 energies owing to the commonly higher CT degree in S_1 state than T_1 state, which leads to a more significant energy reduction of S_1 state and gradually decreased ΔE_{ST} values when environmental polarity rises as doping concentrations increase. Amongst these materials, DPAAP displays the smallest decrease of ΔE_{ST} due to the lowest CT ratio difference between S_1 and T_1 state (Figure S1), along with the lack of inter-CT characteristic as discussed later. Therefore, no delayed fluorescence was detected for DPAAP in doped and neat films (Figure S11). In comparison, similar to TPAAP, both TPAPAP and TPATAP display distinct TADF properties and gradually decreased delayed fluorescence lifetimes (τ_{TADF}) as doping concentration increase (Figures S13 and S15; Tables S4 and S5). Correspondingly, their neat films show very small ΔE_{ST} values of 0.03 and 0.06 eV, and short τ_{TADF} values of 3.2 and 5.1 μs for TPAPAP and TPATAP, respectively, which is beneficial for RISC processes.

Hindered by the energy-gap law, these solid films exhibit gradually decreased PLQY values as emission wavelengths bathochromically shift (Figure 3D). Notably, TPATAP with strong electron-donating thiophene π -bridge displays almost identical PLQY from 700 to 780 nm as TPAAP, and further extends high performance into longer wavelength region ($\lambda_{em} = 788$ nm, PLQY = 18.9% for 60 wt% doped film, and $\lambda_{em} = 834$ nm, PLQY = 4.1% for neat film), which are among the highest values for the reported NIR-TADF materials in the same spectral range.^[25–27,40–45] In order to understand their large PLQY difference in solid state, we plotted their variation trends of k_r and k_{nr} (Figure 3E,F). For DPAAP and TPAAP, their k_r values are quite similar, while the rapidly increased k_{nr} in DPAAP results in about 40% decreased PLQYs in absolute value in the same spectra region. Compared with TPAAP, TPAPAP shows ≈20–30% reduced PLQYs in absolute value due to rapidly decreased k_r values above 700 nm, albeit their k_{nr} values are quite similar. For TPATAP, although its k_{nr} values are larger than those of TPAAP and TPAPAP, its k_r values are the highest and are significantly larger than those of the other three materials. To summarize, although these compounds all possess high PLQYs above 90% in oxygen-free toluene solutions at single-molecule level, their emission performance varies greatly in solid films, demonstrating significant impact of aggregation behavior.

2.4 | Experimental validation of inter-CT states

To confirm the existence of inter-CT states in solid films, we first performed transient absorption (TA) measurements. DPAAP and TPATAP neat films showed similar characteristic TA peaks below 950 nm (Figure 4A,B). The positive

bands at \approx 450–500, 650–700, and 850–950 nm are excited state absorptions (ESA). The negative band at \approx 550–600 nm is ground state bleaching (GSB), in accordance with their steady-state absorption. However, different from DPAAP, TPATAP neat film displayed another broad and structureless ESA band above 1000 nm, which was also observed in TPAAP and TPAPAP neat films (Figure S16). Furthermore, compared with DPAAP neat film, DPAAP:PC₆₀BM 1:1 blend film generated a new ESA peak above 1000 nm (Figure S17), indicating electron transfer from DPAAP to strong electron acceptor PC₆₀BM.^[24] More notably, such ESA peak in TPAAP, TPAPAP and TPATAP blend films with PC₆₀BM were significantly strengthened relative to their neat films, indicating more efficient inter-CT processes with the addition of PC₆₀BM. Thus, the ESA peak above 1000 nm could be assigned to hole polarons photo-induced absorption (PIA) on dopants with inter-CT characteristics, confirming the existence of inter-CT in TPAAP, TPAPAP and TPATAP neat films. In comparison, DPAAP neat films only display intra-CT characteristic.

We also performed time-resolved PL (TRPL) measurements. For DPAAP neat films (Figure 4C), its PL spectra first shows a slight redshift \approx 14 nm within the timescale of 0.5 ns and then keeps unchanged. Meanwhile, its decay profile at different wavelength has a similar lifetime with single-exponential characteristic (Figure 4E), demonstrating the existence of only intra-CT species.^[46] For sharp comparison, TRPL of TPATAP neat film demonstrates a gradual and distinct bathochromic shift \approx 40 nm within the first 2 ns (Figure 4D). Furthermore, its decay profile exhibited a dependence on emission wavelengths, indicating the existence of different emission species. At shorter wavelength of 730 nm, there are two kinetic components with a short lifetime of 210 ps and a long lifetime of 1.80 ns. At longer wavelength of 890 nm, there only exist one long lifetime component of 1.92 ns (Figure 4F). Similar phenomena were also observed in TPAAP and TPAPAP neat films (Figure S18). The significant bathochromic shift together with different decay profiles at different wavelengths not only confirm the existence of inter-CT states, but also manifest rapid transformation from high energy intra-CT dominated species to low energy inter-CT dominated species.^[25,47] Moreover, organic solar cells (OSCs) based on TPAAP, TPAPAP and TPATAP neat film displayed power conversion efficiency (PCE) of 0.27%, 0.24% and 0.14% (Figure S19), which is similar to that of BF2 system^[24] with inter-CT property. These values are three orders of magnitudes higher than that based on DPAAP (0.0004%). Therefore, through these comprehensive experiments, inter-CT characteristic in TPAAP, TPAPAP and TPATAP, and intra-CT characteristic in DPAAP have been explicitly verified.

2.5 | Emission mechanisms

To gain insights into different aggregation effect at solid-state level, we first performed theoretical calculations on nearest-neighbor dimers extracted from the single crystal of all compounds. The configuration of those dimers and the calculated results are summarized in Figures S20 to S23 and Tables S6 to S9. Among those dimers, DPAAP-D1 with acceptors packed in face-to-face manner possesses the

lowest S₁ state energy, while TPAAP-D1, TPAPAP-D1 and TPATAP-D1 with donor of one molecule close to acceptor of the other molecule exhibit the lowest E_{S1}. We further examined the nature of excited states based on these four dimers by visualizing their hole and electron distributions in Multiwfns program.^[48] As shown in Figure 5A, the S₁ state of DPAAP-D1 still keeps intra-CT characteristic. The absence of inter-CT in DPAAP-D1 could be attributed to the shorter d_{h/e} of 3.220 Å in intra-CT state than that of 4.533 Å in inter-CT state (Figure S24). The lower E_{S1} in dimer relatively to single molecule may be due to significant $\pi\cdots\pi$ attractive interactions between the planar acceptor parts of DPAAP monomers.

In contrast, the S₁ states of TPAAP-D1, TPAPAP-D1 and TPATAP-D1 are all of inter-CT characteristic (Figure 5A,B) due to their shorter d_{h/e} values in dimers, leading to a significant reduction of S₁ state energy and ΔE_{ST} values compared with their single molecules (Tables S2, S7–S9), which is similar to our previous work.^[25–27] However, inter-CT type transitions with inherently spatially separated hole and electron will lead to largely decreased f values, that is, 0.0033 for TPAAP-D1, 0.0134 for TPAPAP-D1 and almost zero for TPATAP-D1, respectively, demonstrating unfavorable impact on radiation processes inherited from typical inter-CT species. However, the k_r values of TPAAP and TPATAP neat film are high of 1.01×10^7 and 2.07×10^7 s⁻¹, which are only one tenth of those in toluene solutions (1.41×10^8 and 2.49×10^8 s⁻¹, respectively), indicating f values of dimers calculated based on single crystal structure cannot satisfactorily reflect the experimental results in actual solid film system. That disparity could be attributed to different packing modes and aggregation effect between ordered single crystals and disordered amorphous films.^[43,49–51]

To clarify their inner emission mechanisms and further understand the relationship between aggregate structure and photophysical properties in neat films, we performed molecular dynamics (MD) simulations to mimic their kinetic aggregation behaviors. The center-of-mass (COM) radial distribution functions (RDF) between molecules display amorphous characteristic in all materials without any distinct peak structures (Figure 6A). In the COM RDF between donor and acceptor units (Figure 6B), the sharp peaks correspond to intramolecular COM distances, with values of 0.69, 0.99, 1.25 and 1.18 nm for DPAAP, TPAAP, TPAPAP and TPATAP, respectively. We also calculated average dihedral angle between π -bridge and AP acceptor based on molecular structures from MD simulations, which are 47.0°, 49.2° and 46.6° for TPAAP, TPAPAP and TPATAP, respectively (Figure S26), similar to the results in gas phase. Moreover, there are a certain number of dimers with COM distances below 0.5 nm, indicating the existence of distinct intermolecular D-A interactions in solid films (Figure 6B inset). We extracted these dimers in three categories according to different packing characteristics, that is, A-A type, D-D type and D-A type packing motifs with centroid distance below 0.5 nm, and then calculated the excited state properties of all dimers. Based on “self-doping effect”^[51] that dimers with lower energy will act as dopants and dominate terminal emission, we screened out 20 dimers of each type with the lowest S₁ energy, and summarized their excited-state properties (Tables S10–S21).

For DPAAP, dimers with A-A type packing motifs possess lower E_{S1} values compared with D-A and D-D type

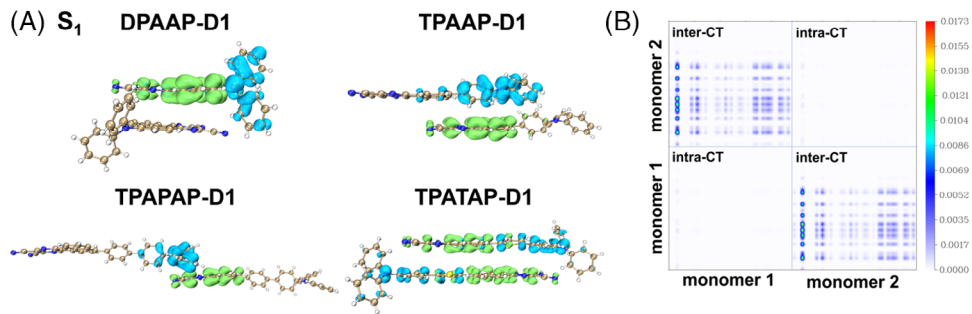


FIGURE 5 (A) Hole and electron distributions of S₁ state in dimers based on single crystal structures. The blue and green isosurfaces (isovalue = 0.0015) represent the hole and electron distributions, respectively. (B) Transition density matrix (TDM) maps of S₁ state in TPATAP-D1. Hydrogen atoms are omitted in TDM due to their little contribution to transitions.

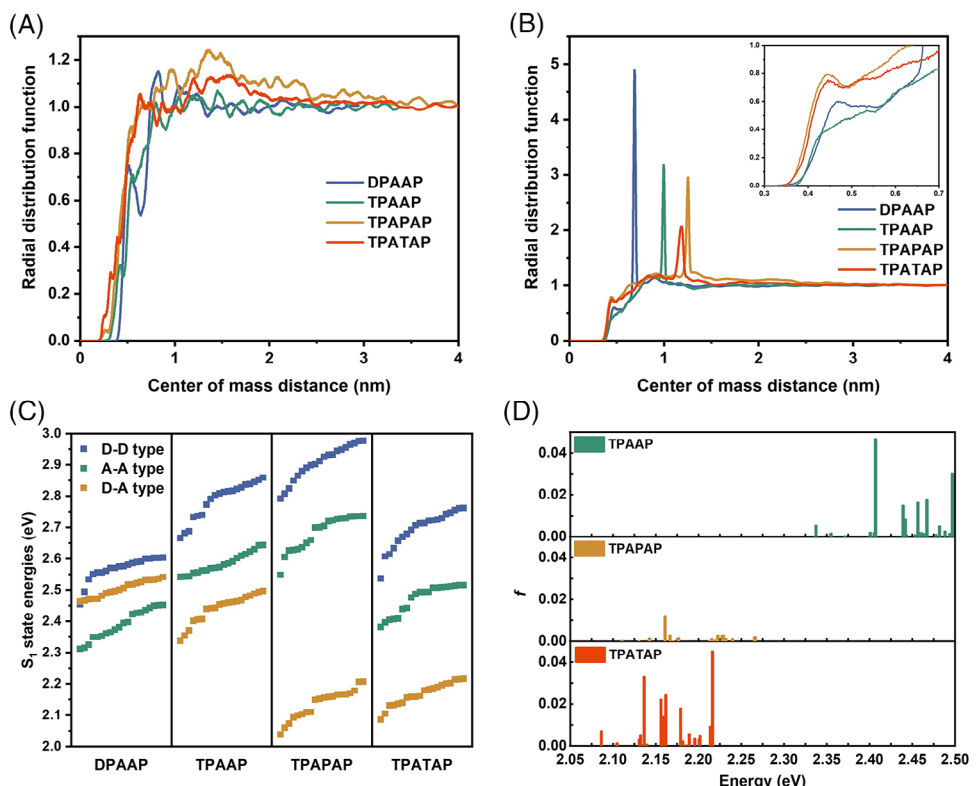


FIGURE 6 (A) Center-of-mass radial distribution functions between molecules. (B) Center-of-mass radial distribution functions between donor and acceptor. (C) Calculated S₁ state energies based on different packing motifs. (D) Distribution of *f* values in TPAAP, TPAPAP and TPATAP D-A type dimers.

(Figure 6C, Tables S10–S12), which could be ascribed to significant $\pi\cdots\pi$ attractive interactions between planar AP acceptors, as evidenced by single crystal structure. Those dimers have relatively large *f* values mostly in the range between 0.10 to 0.37 owing to the fluctuation in D/A dihedral angles, which is typical of intra-CT characteristics. Even for dimers with relatively small *f* values, through the analysis of hole and electron distributions, their S₁ states are also of intra-CT (Figure S27). The lack of inter-CT characteristics in DPAAP dimers accounts for its smallest redshift degree, inactive TADF property and rapid *k*_{nr} increase in solid films, consistent with the above experimental results. In contrast, for TPAAP, TPAPAP and TPATAP, dimers with D-A type packing motifs possess lower *E*_{S₁} due to reduced *d*_{h/e} between intermolecular D and A units, similar to the results based on single crystal structure. Their *f* values in S₁ states are typical

of inter-CT characteristic (Tables S15, S18 and S21). The histogram demonstrates the distribution of *f* values (Figure 6D). The average magnitude of *f* values in TPAAP and TPATAP dimers are distinctly higher than those in TPAPAP dimers, which is in good accordance with experimental results that *k*_{nr} values in TPAAP and TPATAP neat films are markedly higher than that in TPAPAP neat film.

In principle, the excited states calculated by TD-DFT are all adiabatic states, generated from the linear combination of corresponding diabatic states. To shed light on their large disparity in *f* values, Boys-localized diabatization^[52] is performed to explore the specific composition of their adiabatic S₁ states. We choose dimers with the highest *f* in low energy region for each material, that is, TPAAP-DA6, TPAPAP-DA4, and TPATAP-DA5 as examples (Table S22). After diabatization, four lowest diabatic singlet excited states

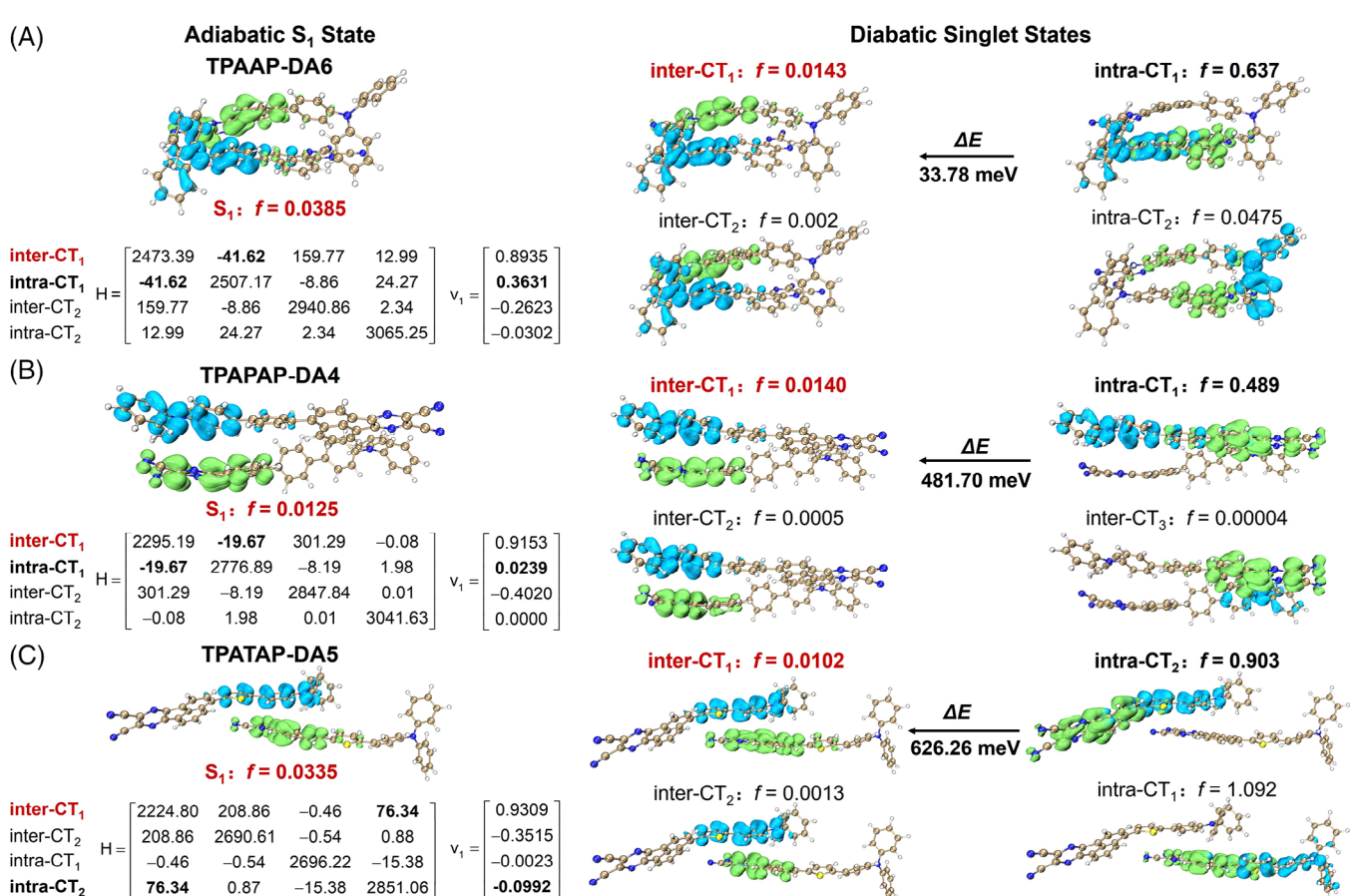


FIGURE 7 The hole and electron distribution of adiabatic S_1 state, the diabatic Hamiltonian and eigenvector v_1 (left side), as well as hole and electron density of the lowest four diabatic singlet excited states (right side) of (A) TPAAP-DA6, (B) TPAPAP-DA4 and (C) TPATAP-DA5, respectively.

with either pure inter-CT or pure intra-CT are constructed (Figure 7A–C). Interestingly, the decomposed lowest diabatic pure inter-CT state of these dimers possesses comparable f values, although their f values in adiabatic inter-CT dominated S_1 state differ greatly. For TPAPAP-DA4, the adiabatic inter-CT state has a similar f to its diabatic pure inter-CT state, while for TPAAP-DA6 and TPATAP-DA5, the adiabatic inter-CT state displays ≈ 3 times f values of their corresponding diabatic pure inter-CT state to 0.0385 and 0.0335, respectively.

Quantificationally, the oscillator strength f could be calculated by the following equation:^[53]

$$f = \frac{2}{3} \Delta E_{fi} \mu_{fi}^2 \quad (2)$$

where ΔE_{fi} is the energy difference between initial and final electronic states (a.u.), and μ_{fi} is transition dipole moment, which is given by:

$$\mu^2 = \mu_x^2 + \mu_y^2 + \mu_z^2 \quad (3)$$

where μ_x , μ_y and μ_z is the component of μ in x , y and z directions. Upon diabatization, we could obtain diabatic Hamiltonian (H) composed of a 4×4 matrix, where diagonal term is the excitation energy of each diabatic state, and non-diagonal term represents electronic couplings between different diabatic states. The eigenvalue λ and eigenvector v of this matrix could be obtained by solving $Hv = \lambda v$, where v

is a 4×1 matrix with the expression of:

$$v_1 = \begin{bmatrix} C_{11} \\ C_{12} \\ C_{13} \\ C_{14} \end{bmatrix}, v_2 = \begin{bmatrix} C_{21} \\ C_{22} \\ C_{23} \\ C_{24} \end{bmatrix}, v_3 = \begin{bmatrix} C_{31} \\ C_{32} \\ C_{33} \\ C_{34} \end{bmatrix}, v_4 = \begin{bmatrix} C_{41} \\ C_{42} \\ C_{43} \\ C_{44} \end{bmatrix} \quad (4)$$

Accordingly, through diabatization, utilizing eigenvector v_1 which is used to build up adiabatic S_1 state, the μ_x in adiabatic S_1 state (denote as $\mu_{x,a}$) could be expressed in linear combinations of μ_x from four diabatic states (denote as $\mu_{xn,d}$, $n = 1\text{--}4$):

$$\mu_{x,a} = C_{11}\mu_{x1,d} + C_{12}\mu_{x2,d} + C_{13}\mu_{x3,d} + C_{14}\mu_{x4,d} \quad (5)$$

$\mu_{y,a}$ and $\mu_{z,a}$ could also be obtained in a similar way. Therefore, large f requires large μ . Considering small μ in diabatic pure inter-CT state and large μ in diabatic pure intra-CT state (Table S22), from diabatic state to adiabatic state, a large coefficient C combined with diabatic pure intra-CT state is essential to a decent f value in adiabatic inter-CT dominated S_1 state. This could be realized by large electronic coupling (\hat{V}) and small energy gap (ΔE) between diabatic inter-CT and intra-CT states.^[54,55]

In general, a large orbital overlap between initial and final state is beneficial for large \hat{V} .^[56,57] In TPAAP-DA6 and TPATAP-DA5, hole distributions of diabatic inter-CT₁ state even spread to AP acceptor part through electron active π -bridge and show large spatial overlap with electron

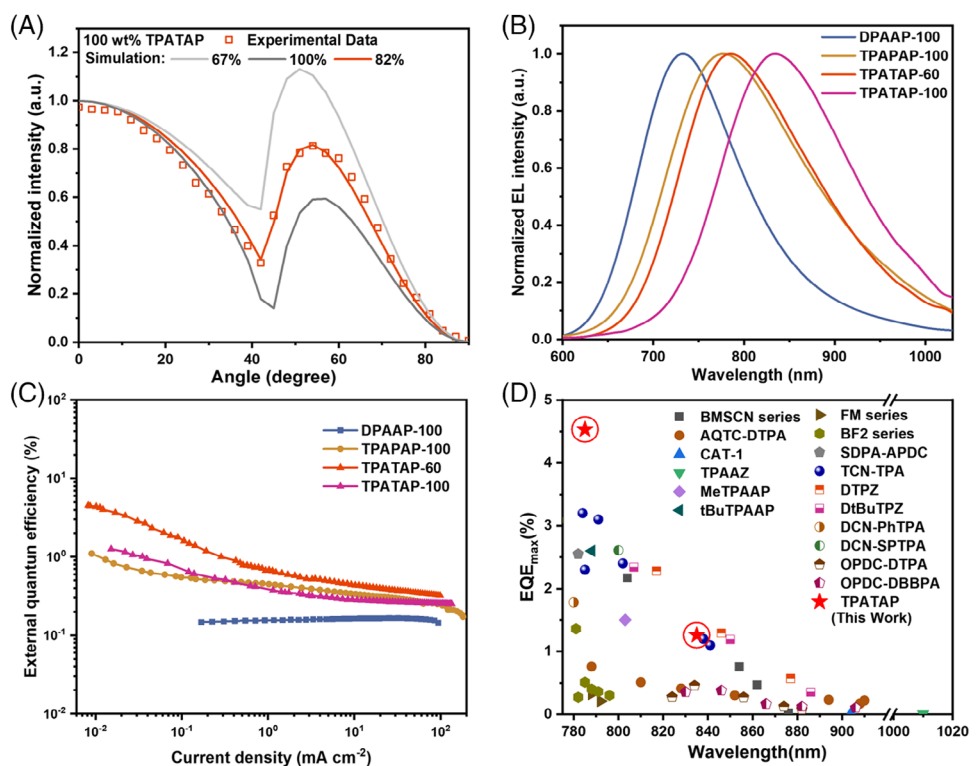


FIGURE 8 (A) Measured *p*-polarized angle-dependent PL intensity at the peak wavelength of TPATAP neat film (Θ_{\parallel} = 100% and 67% correspond to fully horizontal and isotropic dipoles, respectively). (B) EL spectra obtained at current density of 10 mA cm⁻². (C) EQE versus current density curves of different devices. (D) Maximum EQE summary of NIR TADF OLEDs with emission peak above 780 nm.

distribution (Figure 7). But in TPAPAP-DA4, hole distribution of diabatic inter-CT₁ state mostly localizes in TPA part, with very little contribution from phenyl π -bridge due to its lack of electronic functionality. Consequently, for TPAAP-DA6, a sufficient \hat{V} of 41.62 meV and a small ΔE of 33.78 meV between inter-CT₁ and intra-CT₁ diabatic states lead to a large C₁₂ of 0.3631. The large C₁₂ together with large f of 0.637 in intra-CT₁ diabatic state leads to a \approx 2.7 times enhancement in f value from pure inter-CT₁ diabatic state to adiabatic S₁ state. But for TPAPAP-DA4, the \hat{V} value between inter-CT₁ and intra-CT₁ diabatic states is only $-$ 19.67 meV due to the smallest overlap. The small \hat{V} and large ΔE of 481.70 meV result in very small C₁₂ value of 0.0239, indicating negligible interplay between diabatic inter-CT₁ and intra-CT₁ state, which well accords with similar f value between diabatic pure inter-CT₁ state and adiabatic S₁ state. As to TPATAP-DA5, although ΔE between diabatic inter-CT₁ and intra-CT₂ states is the largest (626.26 meV), the \hat{V} value is also the largest (76.34 meV) due to large overlap between hole and electron distribution facilitated by strong electron-donating property of thienyl π -bridge, resulting in a decent C₁₄ of $-$ 0.0992. This C₁₄ value further combines with the largest f of 0.903 in diabatic intra-CT₂ state due to both small dihedral angel and electron-donating property of thienyl π -bridge, leading to \approx 3.3 times enhancement in f value from pure inter-CT₁ diabatic state to adiabatic S₁ state. Therefore, it is the much more effective coupling between diabatic inter-CT and intra-CT states in TPAAP and TPATAP neat films that leads to one order of magnitude larger k_r values than that in TPAPAP neat film, demonstrating great importance of electron-donating π -bridge when designing molecules for achieving high k_r values in solid states.

2.6 | Emitting dipole orientation and electroluminescent properties

Generally, increasing π -conjugation length along molecular long axis would effectively enhance horizontal emitting dipole orientation ratio Θ_{\parallel} , which is beneficial for improving optical outcoupling efficiency (Φ_{out}) in OLEDs. Indeed, as depicted in Figure 8A and Figure S28, D-A type DPAAP without any π -bridge shows a low Θ_{\parallel} of 71% in neat film, while D- π -A type TPAAP displays an enlargement of Θ_{\parallel} to 76%. For TPAPAP and TPATAP with an extra π -bridge, their Θ_{\parallel} values exhibit effective increase to 81% and 82%, respectively, demonstrating significant advantages of π -bridge elongation for enhancing Θ_{\parallel} .

To evaluate the electroluminescent performances of these emitters, we fabricated multilayer OLEDs with following configuration: indium tin oxide (ITO)/1,4,5,8,9,11-hexaaazatriphenylene hexacarbonitrile (HATCN, 5 nm)/1,1-bis[4-[*N,N*-di(*p*-tolyl)amino]phenyl]-cyclohexane (TAPC, 30 nm)/1,3-bis(*N*-carbazolyl)benzene (mCP, 5 nm)/TPBi: *x* wt% DPAAP, TPAPAP or TPATAP (30 nm)/4,6-bis(3,5-di(pyridin-3-yl)phenyl)-2-methylpyrimidine (B3PyMPM, 60 nm)/LiF (1 nm)/Al (150 nm). As shown in Figure 8B,C, non-doped OLED based on DPAAP (device DPAAP-100) displays a maximum EQE of 0.17% with electroluminescence (EL) peak at 732 nm. As the PLQY value is 4.2% in neat film, the faint EQE demonstrates a low exciton utilizing efficiency (EUE) below 25% due to its lack of TADF property. For TPAPAP based non-doped OLED (device TPAPAP-100), although a high EUE could be ensured by TADF mechanism, the relatively low PLQY of 4.1% in neat film limits its EL performance

with a maximum EQE of 1.20% at 778 nm. In contrast, benefited from both TADF property and high PLQYs in solid films, TPATAP based devices demonstrate outstanding performances. In detail, 60 wt% doped OLED (device TPATAP-60) exhibits a maximum EQE of 4.53% with EL peak at 785 nm, and non-doped OLED (device TPATAP-100) exhibited a maximum EQE of 1.26% with EL peak at 835 nm, respectively. These results represent state-of-the-art performances among reported TADF OLEDs with EL peak above 780 nm (Figure 8D).^[23,25,40,41,43–45,47,51,58–60] In addition, the non-doped device of TPATAP displays decent operational lifetime with T_{90} of 74.4 hours at a constant current density of 5 mA cm⁻² (Figure S31).

3 | CONCLUSION

We systematically investigated the regulatory role of π -bridge on photophysical properties of D/A type compounds in single molecule and solid film, providing fresh insight into how interplay between inter-CT and intra-CT in molecular aggregates enables large k_r in inter-CT dominated emission. First, the introduction of π -bridge is of essential importance based on phenylamine type donors. Compared with D-A type molecule DPAAAP showing the worst performance in solid state due to the lack of inter-CT, the introduction of π -bridge in TPAAP, TPAPAP and TPATAP not only bring about enhanced k_r and decreased ΔE_{ST} values in single molecule, but also facilitate distinct inter-CT characteristics in solid films with largely reduced k_{nr} and ΔE_{ST} , thus inducing and enhancing desired TADF for efficient NIR emission.

Second and more importantly, π -bridge mediated coupling between inter-CT and intra-CT could maximize radiative decay for adiabatic inter-CT dominated S_1 states through effective couplings with intrinsic diabatic intra-CT states. In particular for TPATAP, strong electron-donating thiényl π -bridge contributes to not only increased π -conjugation length and high $\Theta_{//}$, but also largely enhanced k_r values owing to large f in single molecule together with strong electronic coupling between inter-CT and intra-CT in aggregates. Consequently, OLEDs based on TPATAP achieved record-high EQEs of 4.53% at 785 nm and 1.26% at 835 nm, respectively, which represents state-of-the-art performances among reported TADF emitters above 780 nm.

The vital π -bridge effect revealed herein could provide valuable guidance on rational molecule design for highly efficient NIR TADF materials. Based on TPA donor, introducing extra functional π -bridge adjacent to acceptor part with strong electron-donating property, such as thiophene, selenophene, furan, pyrrole and their relevant derivatives, could simultaneously realize significant emission redshift, largely enhanced k_r values and increased $\Theta_{//}$ in solid films. Guided by the above-mentioned design strategy, through rationally integrating various D and A blocks, NIR TADF molecular library would be greatly enriched in the near future. It is anticipated the vital π -bridge effect for concerted inter-CT and intra-CT in aggregates presented herein would attenuate the limitation of energy gap law, not only to promote burgeoning developments for high-efficiency NIR emitters, but also to enhance the luminescence efficiency of various inter-CT systems, such as OPV materials for improving light-harvesting process.^[61,62]

AUTHOR CONTRIBUTIONS

Juan Qiao conceived and supervised the project. Jingyi Xu, Jie Xue and Yu Dai synthesized organic compounds used in this study. Jingyi Xu and Yu Dai prepared samples and measured their properties. Jinyuan Zhang performed time-resolved PL and TA measurements. Shaman Li conducted OSC device fabrication and measurements. Chengyu Yao set up methods of operation and data collection on MD simulations. Jingyi Xu carried out quantum-chemical calculations, MD simulations and boys-localized diabatization. Jingyi Xu and Yu Dai carried out OLED fabrication and characterization. Juan Qiao, Jingyi Xu and Yu Dai contributed to the writing of this manuscript. Jiajun Ren discussed the results of boys-localized diabatization and provided valuable feedbacks on the manuscript. Qingyu Meng, Xueliang Wen and Haoyun Shao provided helpful discussions and suggestions. All authors discussed the results and commented on the manuscript.

ACKNOWLEDGMENTS

This work was supported by National Key R & D Program of China (Grant No. 2020YFA0715000) and the National Natural Science Foundation of China (Grant No. 51773109). The authors are very grateful to Prof. Zhigang Shuai and Dr. Qikai Li for the assistance of utilizing Q-Chem program resources. The authors thank Dr. Shaoguang Zhang for the assistance with single crystal XRD measurements and also the Center of High-Performance Computing in Tsinghua University and Tsinghua Xuetang Talents Program for supporting computational resources.

CONFLICT OF INTEREST STATEMENT

The authors declare no conflicts of interest.

ORCID

Juan Qiao  <https://orcid.org/0000-0002-9919-3927>

REFERENCES

- K. P. Goetz, D. Vermeulen, M. E. Payne, C. Kloc, L. E. McNeil, O. D. Jurchescu, *J. Mater. Chem. C* **2014**, *2*, 3065.
- J. Blumberger, *Chem. Rev.* **2015**, *115*, 11191.
- H. J. Wörner, C. A. Arrell, N. Banerji, A. Cannizzo, M. Chergui, A. K. Das, P. Hamm, U. Keller, P. M. Kraus, E. Liberatore, P. Lopez-Tarifa, M. Lucchini, M. Meuwly, C. Milne, J.-E. Moser, U. Rothlisberger, G. Smolentsev, J. Teuscher, J. A. van Bokhoven, O. Wenger, *Struct. Dynam.* **2017**, *4*, 061508.
- D. Shen, W.-C. Chen, M.-F. Lo, C.-S. Lee, *Mater. Today Energy* **2021**, *20*, 100644.
- V. May, O. Kühn, *Charge and Energy Transfer Dynamics in Molecular Systems*, Wiley, Hoboken, NJ **2023**.
- C. W. Tang, S. A. Van Slyke, *Appl. Phys. Lett.* **1987**, *51*, 913.
- K. Jinna, R. Kabe, Z. Lin, C. Adachi, *Nat. Mater.* **2022**, *21*, 338.
- V. Coropceanu, X.-K. Chen, T. Wang, Z. Zheng, J.-L. Brédas, *Nat. Rev. Mater.* **2019**, *4*, 689.
- C. Deibel, T. Strobel, V. Dyakonov, *Adv. Mater.* **2010**, *22*, 4097.
- H. Sirringhaus, *Adv. Mater.* **2014**, *26*, 1319.
- X. Yang, D. Wang, *ACS Appl. Energy Mater.* **2018**, *1*, 6657.
- M. Sarma, K. T. Wong, *ACS Appl. Mater. Interfaces* **2018**, *10*, 19279.
- J. Guo, Y. Zhen, H. Dong, W. Hu, *J. Mater. Chem. C* **2021**, *9*, 16843.
- H. Uoyama, K. Goushi, K. Shizu, H. Nomura, C. Adachi, *Nature* **2012**, *492*, 234.
- V. Jankus, P. Data, D. Graves, C. McGuinness, J. Santos, M. R. Bryce, F. B. Dias, A. P. Monkman, *Adv. Funct. Mater.* **2014**, *24*, 6178.
- Y. Hu, Y.-J. Yu, Y. Yuan, Z.-Q. Jiang, L.-S. Liao, *Adv. Opt. Mater.* **2020**, *8*, 1901917.
- X.-Q. Wang, Y. Hu, Y.-J. Yu, Q.-S. Tian, W.-S. Shen, W.-Y. Yang, Z.-Q. Jiang, L.-S. Liao, *J. Phys. Chem. Lett.* **2021**, *12*, 6034.

18. P. A. M. Dirac, N. H. D. Bohr, *Proc. R. Soc. London, Ser. A* **1927**, *114*, 243.
19. R. Englman, J. Jortner, *Mol. Phys.* **1970**, *18*, 145.
20. A. Zampetti, A. Minotto, F. Cacialli, *Adv. Funct. Mater.* **2019**, *29*, 1807623.
21. H. U. Kim, T. Kim, C. Kim, M. Kim, T. Park, *Adv. Funct. Mater.* **2022**, *33*, 2208082.
22. S. Sharma, A. K. Pal, *J. Mater. Chem. C* **2022**, *10*, 15681.
23. H. Ye, D. H. Kim, X. Chen, A. S. D. Sandanayaka, J. U. Kim, E. Zaborova, G. Canard, Y. Tsuchiya, E. Y. Choi, J. W. Wu, F. Fages, J.-L. Bredas, A. D'Aléo, J.-C. Ribierre, C. Adachi, *Chem. Mater.* **2018**, *30*, 6702.
24. A. J. Gillett, C. Tonnellé, G. Lundi, G. Ricci, M. Catherin, D. M. L. Unson, D. Casanova, F. Castet, Y. Olivier, W. M. Chen, E. Zaborova, E. W. Evans, B. H. Drummond, P. J. Conaghan, L.-S. Cui, N. C. Greenham, Y. Puttisong, F. Fages, D. Beljonne, R. H. Friend, *Nat. Commun.* **2021**, *12*, 6640.
25. J. Xu, Y. Dai, J. Zhang, Z. Jia, Q. Meng, J. Qiao, *Adv. Opt. Mater.* **2024**, *12*, 2300989.
26. J. Xue, Q. Liang, R. Wang, J. Hou, W. Li, Q. Peng, Z. Shuai, J. Qiao, *Adv. Mater.* **2019**, *31*, 1808242.
27. J. Xue, J. Xu, J. Ren, Q. Liang, Q. Ou, R. Wang, Z. Shuai, J. Qiao, *Sci. China Chem.* **2021**, *64*, 1786.
28. H. Wang, J.-X. Chen, Y.-Z. Shi, X. Zhang, L. Zhou, X.-Y. Hao, J. Yu, K. Wang, X.-H. Zhang, *Adv. Mater.* **2024**, *36*, 2307725.
29. T. Hu, Z. Tu, G. Han, Y. Yi, *J. Phys. Chem. C* **2021**, *125*, 1249.
30. W. Wei, Z. Yang, X. Chen, T. Liu, Z. Mao, J. Zhao, Z. Chi, *J. Mater. Chem. C* **2020**, *8*, 3663.
31. L. Yu, M. Shi, Z. Wang, X. Xing, M. Umair Ali, Y. He, H. Meng, *ChemPhysChem* **2021**, *22*, 1684.
32. Q. Zhang, H. Kuwabara, W. J. Potsavage Jr, S. Huang, Y. Hatae, T. Shibata, C. Adachi, *J. Am. Chem. Soc.* **2014**, *136*, 18070.
33. S. Wang, Z. Cheng, X. Song, X. Yan, K. Ye, Y. Liu, G. Yang, Y. Wang, *ACS Appl. Mater. Interfaces* **2017**, *9*, 9892.
34. A. Shang, T. Lu, H. Liu, C. Du, F. Liu, D. Jiang, J. Min, H. Zhang, P. Lu, *J. Mater. Chem. C* **2021**, *9*, 7392.
35. R. S. Mulliken, *J. Chem. Phys.* **1939**, *7*, 14.
36. N. J. Turro, V. Ramamurthy, J. C. Scaiano, *Principles of Molecular Photochemistry: An Introduction*, University Science Books, Melville **2009**.
37. G. N. Lewis, M. Calvin, *Chem. Rev.* **1939**, *25*, 273.
38. L. J. E. Hofer, R. J. Grabenstetter, E. O. Wiig, *J. Am. Chem. Soc.* **1950**, *72*, 203.
39. U. Balijapalli, R. Nagata, N. Yamada, H. Nakanotani, M. Tanaka, A. D'Aléo, V. Placide, M. Mamada, Y. Tsuchiya, C. Adachi, *Angew. Chem. Int. Ed.* **2021**, *60*, 8477.
40. J.-F. Cheng, Z.-H. Pan, K. Zhang, Y. Zhao, C.-K. Wang, L. Ding, M.-K. Fung, J. Fan, *Chem. Eng. J.* **2022**, *430*, 132744.
41. Y. Yu, H. Xing, D. Liu, M. Zhao, H. H. Y. Sung, I. D. Williams, J. W. Y. Lam, G. Xie, Z. Zhao, B. Z. Tang, *Angew. Chem. Int. Ed.* **2022**, *61*, e202204279.
42. D. G. Congrave, B. H. Drummond, P. J. Conaghan, H. Francis, S. T. E. Jones, C. P. Grey, N. C. Greenham, D. Credginton, H. Bronstein, *J. Am. Chem. Soc.* **2019**, *141*, 18390.
43. Q. Liang, J. Xu, J. Xue, J. Qiao, *Chem. Commun.* **2020**, *56*, 8988.
44. J.-F. Liu, X.-Q. Wang, Y.-J. Yu, S.-N. Zou, S.-Y. Yang, Z.-Q. Jiang, L.-S. Liao, *Org. Electron.* **2021**, *91*, 106088.
45. J.-X. Liang, Y. Tang, X. Wang, K. Zhang, Y.-w. Shih, C.-H. Chen, T.-L. Chiu, P. J. Li, J.-H. Lee, C.-K. Wang, C.-C. Wu, J. Fan, *J. Mater. Chem. C* **2023**, *11*, 6981.
46. D. Chen, K. Liu, X. Li, B. Li, M. Liu, X. Cai, Y. Ma, Y. Cao, S.-J. Su, *J. Mater. Chem. C* **2017**, *5*, 10991.
47. D.-H. Kim, A. D'Aléo, X.-K. Chen, A. D. S. Sandanayaka, D. Yao, L. Zhao, T. Komino, E. Zaborova, G. Canard, Y. Tsuchiya, E. Choi, J. W. Wu, F. Fages, J.-L. Brédas, J.-C. Ribierre, C. Adachi, *Nat. Photonics* **2018**, *12*, 98.
48. T. Lu, F. Chen, *J. Comput. Chem.* **2012**, *33*, 580.
49. Y. Shirota, *J. Mater. Chem.* **2005**, *15*, 75.
50. Y.-Z. Shi, K. Wang, S.-L. Zhang, X.-C. Fan, Y. Tsuchiya, Y.-T. Lee, G.-L. Dai, J.-X. Chen, C.-J. Zheng, S.-Y. Xiong, X.-M. Ou, J. Yu, J.-S. Jie, C.-S. Lee, C. Adachi, X.-H. Zhang, *Angew. Chem. Int. Ed.* **2021**, *60*, 25878.
51. J. Xue, J. Xu, Q. Liang, Y. Dai, R. Wang, Y. Yi, J. Qiao, *Adv. Funct. Mater.* **2023**, *33*, 2301312.
52. J. E. Subotnik, S. Yeganeh, R. J. Cave, M. A. Ratner, *J. Chem. Phys.* **2008**, *129*, 244101.
53. N. J. Turro, *Modern Molecular Photochemistry*, University Science Books, Melville **1991**.
54. G. W. Robinson, *J. Chem. Phys.* **1967**, *46*, 572.
55. M. Bixon, J. Jortner, J. W. Verhoeven, *J. Am. Chem. Soc.* **1994**, *116*, 7349.
56. C.-P. Hsu, *Acc. Chem. Res.* **2009**, *42*, 509.
57. Z.-Q. You, C.-P. Hsu, *Int. J. Quantum Chem.* **2014**, *114*, 102.
58. Q. Li, J. Xu, S. Tan, Y. Dai, J. Xue, J. Qiao, *Org. Electron.* **2022**, *110*, 106645.
59. B. Ma, Z. Ding, D. Liu, Z. Zhou, K. Zhang, D. Dang, S. Zhang, S.-J. Su, W. Zhu, Y. Liu, *Chem. Eur. J.* **2023**, *29*, e202301197.
60. H. Wang, K. Wang, J.-X. Chen, X. Zhang, L. Zhou, X.-C. Fan, Y.-C. Cheng, X.-Y. Hao, J. Yu, X.-H. Zhang, *Adv. Funct. Mater.* **2023**, *33*, 2304398.
61. X.-K. Chen, V. Coropceanu, J.-L. Brédas, *Nat. Commun.* **2018**, *9*, 5295.
62. G. Zhang, X.-K. Chen, J. Xiao, P. C. Y. Chow, M. Ren, G. Kupgan, X. Jiao, C. C. S. Chan, X. Du, R. Xia, Z. Chen, J. Yuan, Y. Zhang, S. Zhang, Y. Liu, Y. Zou, H. Yan, K. S. Wong, V. Coropceanu, N. Li, C. J. Brabec, J.-L. Bredas, H.-L. Yip, Y. Cao, *Nat. Commun.* **2020**, *11*, 3943.

SUPPORTING INFORMATION

Additional supporting information can be found online in the Supporting Information section at the end of this article.

How to cite this article: J. Xu, J. Xue, Y. Dai, J. Zhang, J. Ren, C. Yao, S. Li, Q. Meng, X. Wen, H. Shao, J. Qiao, *Aggregate* **2024**, *5*, e634.

<https://doi.org/10.1002/agt2.634>